HHS Public Access

Author manuscript

ACS Appl Mater Interfaces. Author manuscript; available in PMC 2022 February 10.

Published in final edited form as:

ACS Appl Mater Interfaces. 2021 February 10; 13(5): 6349–6358. doi:10.1021/acsami.0c21370.

A Pt(II) Decorated Covalent Organic Framework for Photocatalytic Difluoroalkylation and Oxidative Cyclization Reactions

Zainab Almansaf[†,⊤], **Jiyun Hu**[†,⊤], **Federica Zanca**[‡], **Hamid R. Shahsavari**[#,ℙ,†], **Benjamin Kampmeyer**[†], **Miu Tsuji**[†], **Kartik Maity**[†], **Valerie Lomonte**[†], **Yumi Ha**[†], **Piero Mastrorilli**[§], **Stefano Todisco**[§], **Mourad Benamara**[‖], **Rama Oktavian**[‡], **Arsalan Mirjafari**[⊥], **Peyman Z. Moghadam**[#,‡], **Ahmad R. Khosropour**[#,Δ,†], **Hudson Beyzavi**[#,†]

[†]Department of Chemistry and Biochemistry, University of Arkansas, Fayetteville, Arkansas, 72701, United States.

[‡]Department of Chemical and Biological Engineering, The University of Sheffield, Sheffield, S1 3JD, United Kingdom.

[ℙ]Department of Chemistry, Institute for Advanced Studies in Basic Sciences (IASBS), Zanjan, 45137-66731, Iran.

[§]DICATECh, Politecnico di Bari, I-70125, Bari, Italy.

[‖]Institute for Nano Science and Engineering, University of Arkansas, Fayetteville, Arkansas, 72701, United States.

[⊥]Department of Chemistry and Physics, Florida Gulf Coast University, Fort Myers, Florida, 33965, United States.

[Δ]Department of Chemistry, University of Isfahan, Isfahan, 81746-73441, Iran.

Abstract

A new covalent organic framework (COF) based on imine bonds was assembled from 2-(4-formylphenyl)-5-formylpyridine and 1,3,6,8-tetrakis(4-aminophenyl)pyrene which showed interesting dual-pore structure with high crystallinity. Postmetallation of the COF with Pt occurred selectively at the N donor (imine and pyridyl) in the larger pores. The metalated COF served as an excellent recyclable heterogeneous photocatalyst for decarboxylation difluoroalkylation and oxidative cyclization reactions.

Graphical Abstract

[#]**Corresponding Author** Peyman Z. Moghadam p.moghadam@sheffield.ac.uk (corresponding author of computational section).; Hamid R. Shahsavari shahsavari@iasbs.ac.ir; Ahmad R. Khosropour khosropour@chem.ui.ac.ir; On sabbatical leave from IASBS (H. R. Shahsavari) and University of Isfahan (A. R. Khosropour).; Hudson Beyzavi beyzavi@uark.edu; Website: https://beyzavigroup.uark.edu/.

⊤Authors contributed equally.

Supporting Information

Syntheses, characterization data, and experimental methods. The Supporting Information is available free of charge on the ACS Publications website.

The authors declare no competing financial interests.

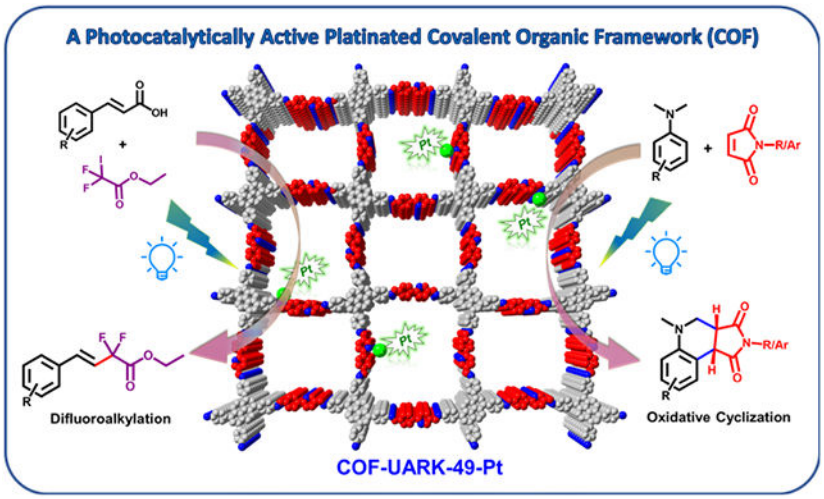

Keywords

covalent organic framework; photocatalysis; difluoroalkylation; oxidative cyclization; platinum; reaction mechanism

Introduction

As a green synthetic route to value-added chemicals, visible light promoted organic transformations have received substantial attention in the past years.[1-3] One of the important research topics is to develop new photocatalysts that are both highly active and stable. Heterogeneous visible light photocatalysts are particularly promising for industrial applications because of the great recyclability compared to homogeneous ones.[4] COFs, an appearing category of crystalline nanoporous polymer material, are found to be an excellent photocatalyst candidate group.[5-8] Firstly, the extended, conjugated framework of COFs provides strong absorption in the visible range. Secondly, the ordered porous structure could facilitate mass, energy, hole, and electron transfer which are critical for photocatalysis. Thirdly, the structure and function of COFs can be tailored in a controllable manner using predesigned molecular linkers enabled by reticular chemistry. These structural features make COFs more promising than inorganic semiconductors.[9-12] The superior photocatalytic performance of COFs has been demonstrated in hydrogen evolution,[13-15] CO_2 reduction,[16-22] and organic transformations.[23-27]

To enhance the photocatalytic efficiency of COF photocatalysts, the engineering of the COF structure has identified some critical factors such as chemical linkage,[28-31] built in donor–acceptor moieties,[16, 32, 33] electronic structure of linkers[13, 34], and so on. Alternatively, doping transition metal atoms into the framework can efficiently modify the photophysical properties of COFs. The *d* orbitals of transition metals offer additional charge transfer process such as ligand-to-metal charge transfer (LMCT) thus further broadening the visible light absorbance of the resulting COFs. Moreover, metal atoms are also able to facilitate electron charge transfer, and inhibit electron and hole recombination.[26, 35-37]

In this work, we introduced 2-(4-formylphenyl)-5-formylpyridine (**L2**) as a COF linker for the first time, complementary to commonly used 2,2'-bipyridine[38-41], porphyrin[42-46], salen, [47-50] and catechol,[51-53] to bind metals. Phenylpyridine derivatives have versatile metal binding modes such as simple pyridine coordination and cyclometallation, which could be an ideal platform to expand the coordination chemistry of COFs. A new stable imine COF was then constructed with 1,3,6,8-tetrakis(4-aminophenyl)pyrene (**L1**) as the amine linker (COF-UARK-49). Post-metalation with platinum leaded to COF-UARK-49-Pt, which displayed excellent photocatalytic performance towards decarboxylative difluoroalkylation and oxidative cyclization reaction.

Experimental Section

Synthesis and experimental procedures including: 1. The synthesis of COF linkers (1,3,6,8-tetrakis(4-aminophenyl)pyrene (**L1**) and 2-(4-formylphenyl)-5-formylpyridine (**L2**)); 2. The synthesis of COFs (COF-UARK-49, COF-UARK-49-Pt, Py-2P COF and Py-2P-Pt) as well as structure simulation are provided in the Supporting Information. The details of photocatalytic reactions including general procedure for difluoroalkylation reaction, general reaction procedure for the oxidative cyclization reaction , and difluoroalkylation reaction with TEMPO are provided in the Supporting Information. All supporting figures, spectroscopic data of the products, and NMR Spectra are also available in the Supporting Information.

Results and Discussions

Synthesis and Characterization.

COF-UARK-49 was synthesized *via* imine condensation of **L1** and **L2** in a mixture solvent of 1,4-dioxane/mesitylene/3M AcOH (1/1/0.2, v/v) at 120 °C for 3 days (Scheme 1, see Supporting Information for details). The successful construction of the imine bond was evidenced by FT-IR spectroscopy and cross-polarization magic-angle-spinning (CP/MAS) solid-state ^{13}C NMR spectroscopy. The IR spectrum of COF-UARK-49 showed the presence of C=N stretching vibrations at 1622 cm^{-1} and the absence of characteristic N–H stretching vibration at 3323cm^{-1} and C=O stretching vibration of at 1738 cm^{-1} of the two linkers respectively (Figure S1). The solid state ^{13}C NMR spectra displayed the characteristic resonance for the imine carbon at 164 ppm (Figure S2). The crystallinity of COF-UARK-49 was investigated by powder X-ray diffraction (PXRD). As presented in Figure 1A, COF-UARK-49 revealed strong diffraction peaks at 2θ = 3.18, 4.90, 6.36, 7.90, and 9.76°, respectively.

To understand the structure of COF-UARK-49, eclipsed and staggered stacking structures which are commonly observed for 2D COFs were modelled in Materials Studio. The eclipsed structure resulted in acceptable consistency with the experimental PXRD patterns (Figure 1A). The interlayer distance deduced from 001 diffraction peak at 2θ = 24° of 3.7 Å is also consistent with the simulated value of 3.8 Å. Interestingly, the simulated AA stacking structure of COF-UARK-49 has two kinds of concave and convex square pores as a result of *cis* orientation of the adjacent imine linkage. The dual-pore structure of COF-UARK-49 was clearly evidenced by nitrogen adsorption–desorption experiment. As depicted in Figure 1B,

COF-UARK-49 showed a type IV isotherm, featuring a sharp uptake below $P/P_0 = 0.01$ and a step between $P/P_0 = 0.10–0.20$, indicating sequential pore filling of two types of pores. Nonlocal density functional theory (NLDFT) calculation showed two narrow pore size distributions at 2.58 nm and 3.06 nm, respectively, assigned to the concave and convex square micropores, respectively (Figure 1C). We also performed grand canonical Monte Carlo (GCMC) simulations of N_2 adsorption in COF-UARK-49 (Figure 2). The simulated isotherm overpredict N_2 uptake specifically in $P/P_0 > 0.1$. This effect could be due to the fact that adsorption simulations are performed on pristine crystal structure whereas in experiments structural defects, pore blockage and/or residual solvents may be present and affect adsorption properties. Importantly, the simulation accurately predicts the position of the isotherm steps at ca. $P/P_0 = 0.01$ and 0.1—indicating sequential pore filling of two types of pores. To further explore this effect, we took a few simulation snapshots from the positioning of N_2 molecules inside the pores at different pressures (Figure 2). The snapshots reveal local ordering of N_2 molecules in the corner of the small pores prior to formation of monolayer within the framework and ultimately pore filling at saturation loadings. The Brunauer–Emmett–Teller (BET) surface area and the total pore volume of COF-UARK-49 were derived to be 1430 $m^2 g^{-1}$ and 0.897 $cm^3 g^{-1}$, respectively. It should be noted that, the isoreticular COF built from 4,4'-biphenyldicarboxaldehyde (Py-2P COF)[54] or 2,2'-bipyridine-5,5'-dicarbaldehyde (Py-2,2'-BPyPh COF)[51] only has one type of pore at around 2.8 nm. The subtle change of the linker structure could be a potential alternative strategy to heteropore COFs[55-57]. Besides, unlike Py-2P COF that quickly lost its crystallinity upon activation due to the disrupted synchronized offset stacking by the twisted biphenyl,[54] COF-UARK-49 is highly stable because of the less twisted nature of 2-phenylpyridine motif compared to biphenyl. Thermogravimetric analysis (TGA) under N_2 proved COF-UARK-49 to be thermally stable up to 480 °C (Figure S3).

2-phenylpyridine derivatives are attractive ligands for transition metals such as Ir and Pt. In particular, Pt(II) complexes are promising photocatalytic centers for both energy transfer and electron transfer process.[58, 59] We therefore firstly explored the Pt binding ability of COF-UARK-49. The platination was conducted by heating *cis*-$[PtCl_2(DMSO)_2]$ and COF-UARK-49 in toluene at 50 °C overnight. The obtained COF-UARK-49-Pt showed identical PXRD pattern to that of COF-UARK-49, suggesting the preservation of crystallinity (Figure 1A). The BET surface area and total pore volume was slightly reduced to 1320 $m^2 g^{-1}$ and 0.774 $cm^3 g^{-1}$ respectively (Figure 1B). The Pt loading was determined to be 9.1% Pt by inductively coupled plasma mass spectrometry (ICP-MS) analysis. Because of the rich metal binding site of COF-UARK-49, various Pt coordinating modes are possible (Figure 3). To understand the coordination environment of Pt inside the framework, we performed both experimental and computational studies. First of all, EDX analysis revealed the relative ratio of Pt/Cl/S was close to 1/2/1 (Figure S4), thus excluding the cyclometallation modes (Figure 3C and 3D) and the chelating binding modes by two nitrogen donors from adjacent COF layers (Figure 3E and 3F) that have been observed for Pd(II)[60]. Thus, only one N donor from the COF (imine or pyridyl N) contributes to the Pt complexation. XPS analysis of the N 1s binding energy revealed that three sub peaks at 397.2, 398.0, 399.2 eV fitted best for COF-UARK-49-Pt, which are assigned to free imine, free pyridyl and Pt coordinated N respectively (Figures 4 and S5). Our attempts to study the potential competing binding by

imine and pyridine nitrogen to Pt of a model compound resulted in ligand decomposition to unidentified products. We therefore used the isoreticular COF constructed from 4,4'-biphenyldicarbaldehyde, Py-2P, that only has imine nitrogen for comparison.39, 54 Platination of Py-2P COF resulted in a Pt loading of 12.5% as determined by ICP-MS for Py-2P-Pt. Py-2P-Pt COF displayed two sub peaks in the N 1s XPS spectrum at binding energy of 398.0 eV for free imine N and 399.0 eV for Pt bonded N respectively (Figure S6). The complex [$PtCl_2$(pyridine)(DMSO)] showed the N 1s binding energy at 399.0 eV (Figure S7). Therefore, it is not conclusive for the Pt coordination environment clarification with XPS analysis. Moreover, DFT calculations revealed that the Gibbs free energy difference of the two structures in Figure 3A and 3B was less than 1 kcal/mol (Table S1). We thus believe that both coordination modes of Figure 3A and 3B could be present in COF-UARK-49-Pt.

Pore size distribution analysis from the nitrogen isotherm revealed a pore size decrease to 2.82 nm and less population of the larger pore compared to COF-UARK-49 while leaving the small concave pore intact (Figure 1C). This indicates that the platination took place exclusively at the convex pores. Based on the Pt loading amount, it is deduced that each of the convex pores is metalated with one platinum. It is also consistent with the experiment finding that using excess platinum precursor did not give higher platinum incorporation. Similar N_2 adsorption behavior was observed for COF-UARK-49-Pt. The morphology of COF-UARK-49 and COF-UARK-49-Pt was studied by scanning electron microscopy (SEM). Both two COFs displayed uniform cubic-like morphology (Figure S8).

COF-UARK-49-Pt as a Photocatalyst for Organic Transformations.

Pyrene based COFs have shown intriguing photophysical properties that can be used for sensing and photocatalysis. The solid-state UV-vis diffuse reflectance spectrum showed that COF-UARK-49 has a broad absorption between 200–600 nm because of increased conjugation compared to the two linkers (Figure 5). Pt incorporation further expands the absorption band to *ca.* 700 nm, covering the whole visible spectrum range, making it an excellent system for visible-light harvesting. The band gap was calculated to be 2.24 and 2.00 eV for COF-UARK-49 and COF-UARK-49-Pt respectively from the UV-vis spectra *via* the Tauc plot (Figures S10), demonstrating the key role of Pt in tuning the band gap. In addition, Pt(II) complexes with vacant axial coordination sites could offer great openings for both inner sphere and outer sphere interactions with substrates. We therefore set to investigate the photocatalytic activity of COF-UARK-49-Pt for the decarboxylative difluoroalkylation and oxidative cyclization reactions, both of which are believed to occur *via* electron transfer pathways.[61-64]

Gem-difluoromethylene group is an important fluorinated moiety broadly present in bioactive and pharmaceutical molecules, *e.g.* Maraviroc (HIV-1 therapeutic agent), Tafluprost (ocular hypertension drug), and Gemcitabine (chemotherapy drug).[65-68] However, using COFs as a (photo)catalyst for fluorination reactions remains to be explored.[69, 70] We utilized COF-UARK-49-Pt to catalyze the decarboxylative difluoroalkylation reaction, which was found to be an efficient method of synthesizing fluorinated compounds. First, we optimized the reaction conditions (Table 1). We found that under the optimized reaction conditions, the model reaction between **1a** and **2** proceeded smoothly to give **3a** in 64%

yield in the presence of COF-UARK-49-Pt, illuminated with a blue LED light (Table 1, entry 2). Control reactions disclosed that both light and photocatalyst were crucial to the reaction efficiency (Table 1, entries 1 and 4). Under similar conditions, COF-UARK-49 gave a much lower yield of 23%, indicating important role of Pt in the framework (Table 1, entry 3). The COF catalyst are recyclable for at least five runs without compromising the efficiency (Figure S11). A wide range of cinnamic acids were readily converted to the corresponding *E*-difluoroacetyl alkenes in good to excellent yields with high *E*/*Z* selectivity using COF-UARK-49-Pt as photocatalyst (Scheme 2). Cinnamic acids bearing both electron-donating (**3d**, **3e**) and -withdrawing (**3g**-**3c**) substituents on the aromatic rings gave good to excellent yield. Halogen substitutions such as fluoro (**3g**) or chloro (**3b**) on the aromatic ring were tolerated without undesired dehalogenation. Nitro substitutions (**3c**) also remained intact during the reaction. The scope of the presented procedure also includes carbocyclic (**3a** and **3f**) and heterocyclic (**3h**) difluorinated systems.

A plausible mechanism for this transformation is illustrated in Scheme 3 according to the literature.[61] Upon COF-UARK-49-Pt light excitation, a single electron transfer (SET) reduction of R_F-I by excited [COF-UARK-49-Pt]* generates one electron-oxidized species $[COF\text{-}UARK\text{-}49\text{-}Pt]^+$ and radical $^{\bullet}R_F$ which reacts with the deprotonated α,β-vinyl carboxylate to generate **I** as a benzylic radical species. Its subsequent oxidation by $[COF\text{-}UARK\text{-}49\text{-}Pt]^+$ generates carboxyl radical intermediate **II** which furnishes the desired product with high *E* selectivity *via* decarboxylation. The generation of $^{\bullet}R_F$ radical during the reaction was demonstrated in a trapping experiment. In the presence of TEMPO as a radical inhibitor, no difluoroacetyl alkenes product was obtained, and TEMPO-trapped difluoroacetyl product was observed instead (Figure S12).

Motivated by the successful decarboxylation-difluoroalkylation, we extended our investigation on the photo-oxidative cyclization reaction using COF-UARK-49-Pt (Scheme 4). After optimization of the reaction conditions, we were pleased to find that COF-UARK-49-Pt readily catalyzed the reaction, giving **6a** in 66% yield (Table S2). Likewise, a series of control experiments proved that COF-UARK-49-Pt was superior to COF-UARK-49, emphasizing the importance of Pt within the COF (Table S2). The involvement of O_2 in the reaction was confirmed by the low yield (7%, Table S2) when the reaction occurred under N_2 atmosphere. As illustrated in Scheme 4, substrates with electron withdrawing groups, *i.e.*, −F (**4b**), −Br (**4c** and **4d)** are compatible with this protocol and the anticipated products were obtained in good to excellent yields (66–85%). It is worth noting that 3-fluoro-*N*,*N*-dimthylaniline provides two isomers with almost equal ratio (Scheme 4, **6b**). 1-*N*,*N*-dimethylaminonaphthalene produced the corresponding product in an excellent yield (82%, **6e**). On the other hand, by using *N*-methylmaleimide instead of *N*-phenylmaleimide, the desired products were obtained in 78% and 85% (**6f** and **6g**), respectively. The recyclability of COF-UARK-49-Pt was also evaluated for oxidative cyclization reaction. The COF catalyst can be reused for at least ten runs without any notable loss of its catalytic performance (Figures S13 and S14).

Based on literature reports,[62-64] a plausible mechanism for the photo-induced oxidative cyclization is shown in Scheme 5. An SET from **I** to [COF-UARK-49-Pt]* generates the amine radical cation **II**, while [COF-UARK-49-Pt]* is reduced to the $[COF\text{-}UARK\text{-}49\text{-}Pt]^-$.

In the presence of oxygen, the photoredox catalytic cycle of COF-UARK-49-Pt is completed via an SET oxidation, with the generation of a superoxide radical anion $O_2^{\bullet-}$. Deprotonation of **II** produces α-aminoalkyl radical **III**. Then **III** reacts with **IV** to generate radical **V**, and the latter then undergoes cyclization to form intermediate **VI**. Proton and electron transfer from **VI** to $O_2^{\bullet-}$ yields the final product **VII** and HOO^-. The HOO^- will be afterwards protonated to yield H_2O_2 as the by-product. The significant inhibition of the reaction in the presence of KI as a hole scavenger, $AgNO_3$ as an electron scavenger and 1,4-benzoquinone as a $O_2^{\bullet-}$ radical scavenger supports the proposed mechanism (Table S2).

Conclusion

In summary, we reported here a pyrene-based imine COF with the incorporation of 2-phenylpyridine as a new metal binding group on the pore wall. The COF-UARK-49 adopted an unprecedented hetero-pore structure that results from the cis orientation of the C=N linkages. It also showed selective metalation (Pt) of the larger pores and enhanced photocatalytic performance in decarboxylative difluoroalkylation and oxidative cyclization reactions after Pt loading. Although imine and pyridyl *N* had similar stabilization effect for Pt in this work, the well-known cyclometallation chemistry of 2-phenylpyridine derivatives could introduce interesting metallacycles decorated COFs if other metals are used (e.g. Ir).

Supplementary Material

Refer to Web version on PubMed Central for supplementary material.

ACKNOWLEDGMENT

H.B. gratefully acknowledges the financial support through the startup funds from the University of Arkansas and the NIH-NIGMS (GM132906). R.O would like to acknowledge funding support during his Ph.D study from Indonesian Endowment Fund for Education-LPDP with the contract No. 202002220216006.

REFERENCES

1. Marzo L; Pagire SK; Reiser O; König B, Visible-Light Photocatalysis: Does It Make a Difference in Organic Synthesis? Angew. Chem. Int. Ed 2018, 57, 10034–10072.
2. Schultz DM; Yoon TP, Solar Synthesis: Prospects in Visible Light Photocatalysis. Science 2014, 343, 1239176. [PubMed: 24578578]
3. Yoon TP; Ischay MA; Du J, Visible Light Photocatalysis as a Greener Approach to Photochemical Synthesis. Nat. Chem 2010, 2, 527–532. [PubMed: 20571569]
4. Lang X; Chen X; Zhao J, Heterogeneous Visible Light Photocatalysis for Selective Organic Transformations. Chem. Soc. Rev 2014, 43, 473–486. [PubMed: 24162830]
5. Geng K; He T; Liu R; Tan KT; Li Z; Tao S; Gong Y; Jiang Q; Jiang D, Covalent Organic Frameworks: Design, Synthesis, and Functions. Chem. Rev 2020, 120, 8814–8933. [PubMed: 31967791]
6. Lohse MS; Bein T, Covalent Organic Frameworks: Structures, Synthesis, and Applications. Adv. Funct. Mater 2018, 28, 1705553.
7. Diercks CS; Yaghi OM, The Atom, the Molecule, and the Covalent Organic Framework. Science 2017, 355, eaal1585. [PubMed: 28254887]
8. Tao S; Jiang D, Covalent Organic Frameworks for Energy Conversions: Current Status, Challenges, and Perspectives. CCS Chem. 2020, 2, 2003–2024.

9. Li X; Zhang J; Huo Y; Dai K; Li S; Chen S, Two-Dimensional Sulfur- and Chlorine-Codoped g-C_3N_4/CdSe-Amine Heterostructures Nanocomposite with Effective Interfacial Charge Transfer and Mechanism Insight. Appl. Catal. B Environ 2021, 280, 119452.
10. Huo Y; Zhang J; Dai K; Li Q; Lv J; Zhu G; Liang C, All-Solid-State Artificial Z-Scheme Porous g-C3N4/Sn2S3-DETA Heterostructure Photocatalyst with Enhanced Performance in Photocatalytic CO_2 Reduction. Appl. Catal. B Environ 2019, 241, 528–538.
11. Lv J; Zhang J; Liu J; Li Z; Dai K; Liang C, Bi SPR-Promoted Z-Scheme Bi2MoO6/CdS-Diethylenetriamine Composite with Effectively Enhanced Visible Light Photocatalytic Hydrogen Evolution Activity and Stability. *ACS Sustain*. Chem. Eng 2018, 6, 696–706.
12. Asahi R; Morikawa T; Irie H; Ohwaki T, Nitrogen-Doped Titanium Dioxide as Visible-Light-Sensitive Photocatalyst: Designs, Developments, and Prospects. Chem. Rev 2014, 114, 9824–9852. [PubMed: 25216232]
13. Vyas VS; Haase F; Stegbauer L; Savasci G; Podjaski F; Ochsenfeld C; Lotsch BV, A Tunable Azine Covalent Organic Framework Platform for Visible Light-Induced Hydrogen Generation. Nat. Commun 2015, 6, 8508. [PubMed: 26419805]
14. Wang X; Chen L; Chong SY; Little MA; Wu Y; Zhu W-H; Clowes R; Yan Y; Zwijnenburg MA; Sprick RS; Cooper AI, Sulfone-Containing Covalent Organic Frameworks for Photocatalytic Hydrogen Evolution from Water. Nat. Chem 2018, 10, 1180–1189. [PubMed: 30275507]
15. Stegbauer L; Schwinghammer K; Lotsch BV, A Hydrazone-Based Covalent Organic Framework for Photocatalytic Hydrogen Production. Chem. Sci 2014, 5, 2789–2793.
16. Jin E; Lan Z; Jiang Q; Geng K; Li G; Wang X; Jiang D, 2D sp^2 Carbon-Conjugated Covalent Organic Frameworks for Photocatalytic Hydrogen Production from Water. Chem 2019, 5, 1632–1647.
17. Yang S; Hu W; Zhang X; He P; Pattengale B; Liu C; Cendejas M; Hermans I; Zhang X; Zhang J, 2D Covalent Organic Frameworks as Intrinsic Photocatalysts for Visible Light-Driven CO_2 Reduction. J. Am. Chem. Soc 2018, 140, 14614–14618. [PubMed: 30352504]
18. Popov DA; Luna JM; Orchanian NM; Haiges R; Downes CA; Marinescu SC, A 2,2′ -Bipyridine-Containing Covalent Organic Framework Bearing Rhenium(I) Tricarbonyl Moieties for CO_2 Reduction. Dalton Trans. 2018, 47, 17450–17460. [PubMed: 30499569]
19. Deng X; Qin Y; Hao M; Li Z, MOF-253-Supported Ru Complex for Photocatalytic CO_2 Reduction by Coupling with Semidehydrogenation of 1,2,3,4-Tetrahydroisoquinoline (THIQ). Inorg. Chem 2019, 58, 16574–16580. [PubMed: 31774657]
20. Deng X; Albero J; Xu L; García H; Li Z, Construction of a Stable Ru–Re Hybrid System Based on Multifunctional MOF-253 for Efficient Photocatalytic CO_2 Reduction. Inorg. Chem 2018, 57, 8276–8286. [PubMed: 29965734]
21. Sun D; Gao Y; Fu J; Zeng X; Chen Z; Li Z, Construction of a Supported Ru Complex on Bifunctional MOF-253 for Photocatalytic CO_2 Reduction under Visible Light. Chem. Commun 2015, 51, 2645–2648.
22. Zhou T; Du Y; Borgna A; Hong J; Wang Y; Han J; Zhang W; Xu R, Post-Synthesis Modification of a Metal–Organic Framework to Construct a Bifunctional Photocatalyst for Hydrogen Production. Energy Environ. Sci 2013, 6, 3229–3234.
23. Zhang T; Xing G; Chen W; Chen L, Porous Organic Polymers: A Promising Platform for Efficient Photocatalysis. Mater. Chem. Front 2020, 4, 332–353.
24. Wang G-B; Li S; Yan C-X; Zhu F-C; Lin Q-Q; Xie K-H; Geng Y; Dong Y-B, Covalent Organic Frameworks: Emerging High-Performance Platforms for Efficient Photocatalytic Applications. J. Mater. Chem. A 2020, 8, 6957–6983.
25. Guo LP; Jin SB, Stable Covalent Organic Frameworks for Photochemical Applications. ChemPhotoChem 2019, 3, 973–983.
26. Wang H; Wang H; Wang Z; Tang L; Zeng G; Xu P; Chen M; Xiong T; Zhou C; Li X; Huang D; Zhu Y; Wang Z; Tang J, Covalent Organic Framework Photocatalysts: Structures and Applications. Chem. Soc. Rev. 2020, 49, 4135–4165. [PubMed: 32421139]
27. Yang Q; Luo M; Liu K; Cao H; Yan H, Covalent Oganic Frameworks for Photocatalytic Applications. Appl. Catal. B Environ 2020, 276, 119174.

28. Li S; Li L; Li Y; Dai L; Liu C; Liu Y; Li J; Lv J; Li P; Wang B, Fully Conjugated Donor–Acceptor Covalent Organic Frameworks for Photocatalytic Oxidative Amine Coupling and Thioamide Cyclization. ACS Catal. 2020, 10, 8717–8726.
29. Chen R; Shi J-L; Ma Y; Lin G; Lang X; Wang C, Designed Synthesis of a 2D Porphyrin-Based sp^2 Carbon-Conjugated Covalent Organic Framework for Heterogeneous Photocatalysis. Angew. Chem. Int. Ed 2019, 58, 6430–6434.
30. Mo C; Yang M; Sun F; Jian J; Zhong L; Fang Z; Feng J; Yu D, Alkene-Linked Covalent Organic Frameworks Boosting Photocatalytic Hydrogen Evolution by Efficient Charge Separation and Transfer in the Presence of Sacrificial Electron Donors. Adv. Sci 2020, 1902988.
31. Wang H; Qian C; Liu J; Zeng Y; Wang D; Zhou W; Gu L; Wu H; Liu G; Zhao Y, Integrating Suitable Linkage of Covalent Organic Frameworks into Covalently Bridged Inorganic/Organic Hybrids toward Efficient Photocatalysis. J. Am. Chem. Soc 2020, 142, 4862–4871. [PubMed: 32073853]
32. Ghosh S; Nakada A; Springer MA; Kawaguchi T; Suzuki K; Kaji H; Baburin I; Kuc A; Heine T; Suzuki H; Abe R; Seki S, Identification of Prime Factors to Maximize the Photocatalytic Hydrogen Evolution of Covalent Organic Frameworks. J. Am. Chem. Soc 2020, 142, 9752–9762. [PubMed: 32352795]
33. Wang G-B; Li S; Yan C-X; Lin Q-Q; Zhu F-C; Geng Y; Dong Y-B, A Benzothiadiazole-Based Covalent Organic Framework for Highly Efficient Visible-Light Driven Hydrogen Evolution. Chem. Commun 2020, 56, 12612–12615.
34. Chen W; Wang L; Mo D; He F; Wen Z; Wu X; Xu H; Chen L, Modulating Benzothiadiazole-Based Covalent Organic Frameworks via Halogenation for Enhanced Photocatalytic Water Splitting. Angew. Chem. Int. Ed 2020, 59, 16902–16909.
35. Chen J; Tao X; Tao L; Li H; Li C; Wang X; Li C; Li R; Yang Q, Novel Conjugated Organic Polymers as Candidates for Visible-Light-Driven Photocatalytic Hydrogen Production. Appl. Catal. B Environ 2019, 241, 461–470.
36. Zhang Y; Hu Y; Zhao J; Park E; Jin Y; Liu Q; Zhang W, Covalent Organic Framework-Supported Fe–TiO_2 Nanoparticles as Ambient-Light-Active Photocatalysts. J. Mater. Chem. A 2019, 7, 16364–16371.
37. Dong Z; Zhang L; Gong J; Zhao Q, Covalent Organic Framework Nanorods Bearing Single Cu Sites for Efficient Photocatalysis. Chem. Eng. J 403, 126383.
38. Sun Q; Aguila B; Perman J; Nguyen N; Ma S, Flexibility Matters: Cooperative Active Sites in Covalent Organic Framework and Threaded Ionic Polymer. J. Am. Chem. Soc 2016, 138, 15790–15796. [PubMed: 27934007]
39. Leng W; Peng Y; Zhang J; Lu H; Feng X; Ge R; Dong B; Wang B; Hu X; Gao Y, Sophisticated Design of Covalent Organic Frameworks with Controllable Bimetallic Docking for a Cascade Reaction. Chem. Eur. J 2016, 22, 9087–9091. [PubMed: 27124832]
40. Aiyappa HB; Thote J; Shinde DB; Banerjee R; Kurungot S, Cobalt-Modified Covalent Organic Framework as a Robust Water Oxidation Electrocatalyst. Chem. Mater 2016, 28, 4375–4379.
41. Zhong W; Sa R; Li L; He Y; Li L; Bi J; Zhuang Z; Yu Y; Zou Z, A Covalent Organic Framework Bearing Single Ni Sites as a Synergistic Photocatalyst for Selective Photoreduction of CO_2 to CO. J. Am. Chem. Soc 2019, 141, 7615–7621. [PubMed: 30998334]
42. Lin S; Diercks CS; Zhang Y-B; Kornienko N; Nichols EM; Zhao Y; Paris AR; Kim D; Yang P; Yaghi OM; Chang CJ, Covalent Organic Frameworks Comprising Cobalt Porphyrins for Catalytic CO_2 Reduction in Water. Science 2015, 349, 1208–1213. [PubMed: 26292706]
43. Chen X; Addicoat M; Jin E; Zhai L; Xu H; Huang N; Guo Z; Liu L; Irle S; Jiang D, Locking Covalent Organic Frameworks with Hydrogen Bonds: General and Remarkable Effects on Crystalline Structure, Physical Properties, and Photochemical Activity. J. Am. Chem. Soc 2015, 137, 3241–3247. [PubMed: 25706112]
44. Wang H; Ding H; Meng X; Wang C, Two-Dimensional Porphyrin- and Phthalocyanine-Based Covalent Organic Frameworks. Chin. Chem. Lett 2016, 27, 1376–1382.
45. Lin G; Ding H; Chen R; Peng Z; Wang B; Wang C, 3D Porphyrin-Based Covalent Organic Frameworks. J. Am. Chem. Soc 2017, 139, 8705–8709. [PubMed: 28595005]

46. Meng Y; Luo Y; Shi JL; Ding H; Lang X; Chen W; Zheng A; Sun J; Wang C, 2D and 3D Porphyrinic Covalent Organic Frameworks: The Influence of Dimensionality on Functionality. Angew. Chem. Int. Ed 2020, 59, 3624–3629.
47. Li L-H; Feng X-L; Cui X-H; Ma Y-X; Ding S-Y; Wang W, Salen-Based Covalent Organic Framework. J. Am. Chem. Soc 2017, 139, 6042–6045. [PubMed: 28385018]
48. Han X; Xia Q; Huang J; Liu Y; Tan C; Cui Y, Chiral Covalent Organic Frameworks with High Chemical Stability for Heterogeneous Asymmetric Catalysis. J. Am. Chem. Soc. 2017, 139, 8693–8697. [PubMed: 28595384]
49. Yuan G; Jiang H; Zhang L; Liu Y; Cui Y, Metallosalen-Based Crystalline Porous Materials: Synthesis and Property. Coord. Chem. Rev 2019, 378, 483–499.
50. Yan S; Guan X; Li H; Li D; Xue M; Yan Y; Valtchev V; Qiu S; Fang Q, Three-dimensional Salphen-based Covalent–Organic Frameworks as Catalytic Antioxidants. J. Am. Chem. Soc 2019, 141, 2920–2924. [PubMed: 30717592]
51. Chen X; Huang N; Gao J; Xu H; Xu F; Jiang D, Towards Covalent Organic Frameworks with Predesignable and Aligned Open Docking Sites. Chem. Commun 2014, 50, 6161–6163.
52. Zhang W; Jiang P; Wang Y; Zhang J; Gao Y; Zhang P, Bottom-up Approach to Engineer a Molybdenum-Doped Covalent-Organic Framework Catalyst for Selective Oxidation Reaction. RSC Adv. 2014, 4, 51544–51547.
53. Vardhan H; Verma G; Ramani S; Nafady A; Al-Enizi AM; Pan Y; Yang Z; Yang H; Ma S, Covalent Organic Framework Decorated with Vanadium as a New Platform for Prins Reaction and Sulfide Oxidation. ACS Appl. Mater. Interfaces 2019, 11, 3070–3079. [PubMed: 30585715]
54. Auras F; Ascherl L; Hakimioun AH; Margraf JT; Hanusch FC; Reuter S; Bessinger D; Döblinger M; Hettstedt C; Karaghiosoff K; Herbert S; Knochel P; Clark T; Bein T, Synchronized Offset Stacking: A Concept for Growing Large-Domain and Highly Crystalline 2D Covalent Organic Frameworks. J. Am. Chem. Soc 2016, 138, 16703–16710. [PubMed: 27992179]
55. Liang R-R; Zhao X, Heteropore Covalent Organic Frameworks: A New Class of Porous Organic Polymers with Well-Ordered Hierarchical Porosities. Org. Chem. Front. 2018, 5, 3341–3356.
56. Liang R-R; Jiang S-Y; A R-H; Zhao X, Two-Dimensional Covalent Organic Frameworks with Hierarchical Porosity. Chem. Soc. Rev 2020, 49, 3920–3951. [PubMed: 32427238]
57. Jin Y; Hu Y; Zhang W, Tessellated Multiporous Two-Dimensional Covalent Organic Frameworks. Nat. Rev. Chem 2017, 1, 0056.
58. Casado-Sánchez A; Gómez-Ballesteros R; Tato F; Soriano FJ; Pascual-Coca G; Cabrera S; Alemán J, Pt(II) Coordination Complexes as Visible Light Photocatalysts for the Oxidation of Sulfides Using Batch and Flow Processes. Chem. Commun 2016, 52, 9137–9140.
59. López-Magano A; Platero-Prats AE; Cabrera S; Mas-Ballesté R; Alemán J, Incorporation of Photocatalytic Pt(II) Complexes into Imine-Based Layered Covalent Organic Frameworks (COFs) Through Monomer Truncation Strategy. Appl. Catal. B Environ 2020, 272, 119027.
60. Ding S-Y; Gao J; Wang Q; Zhang Y; Song W-G; Su C-Y; Wang W, Construction of Covalent Organic Framework for Catalysis: Pd/COF-LZU1 in Suzuki–Miyaura Coupling Reaction. J. Am. Chem. Soc 2011, 133, 19816–19822. [PubMed: 22026454]
61. Zhong JJ; Yang C; Chang XY; Zou C; Lu W; Che CM, Platinum(II) Photo-Catalysis for Highly Selective Difluoroalkylation Reactions. Chem. Commun 2017, 53, 8948–8951.
62. Liang Z; Xu S; Tian W; Zhang R, Eosin Y-Catalyzed Visible-Light-Mediated Aerobic Oxidative Cyclization of N,N-Dimethylanilines with Maleimides. Beilstein J. Org. Chem 2015, 11, 425–430. [PubMed: 25977716]
63. Yang X-L; Guo J-D; Lei T; Chen B; Tung C-H; Wu L-Z, Oxidative Cyclization Synthesis of Tetrahydroquinolines and Reductive Hydrogenation of Maleimides under Redox-Neutral Conditions. Org. Lett 2018, 20, 2916–2920. [PubMed: 29737179]
64. Nicholls TP; Constable GE; Robertson JC; Gardiner MG; Bissember AC, Bronsted Acid Cocatalysis in Copper(I)-Photocatalyzed alpha-Amino C-H Bond Functionalization. ACS Catal. 2016, 6, 451–457.
65. Müller K; Faeh C; Diederich F, Fluorine in Pharmaceuticals: Looking Beyond Intuition. Science 2007, 317, 1881–1886. [PubMed: 17901324]

66. O'Hagan D, Understanding Organofluorine Chemistry. An Introduction to the C–F Bond. Chem. Soc. Rev 2008, 37, 308–319. [PubMed: 18197347]

67. Chen B; Vicic DA, Transition-Metal-Catalyzed Difluoromethylation, Difluoromethylenation, and Polydifluoromethylenation Reactions In Organometallic Fluorine Chemistry, Braun T; Hughes RP, Eds. Springer International Publishing: Cham, 2015; pp 113–141.

68. Wang Z; Guo C-Y; Yang C; Chen J-P, Ag-Catalyzed Chemoselective Decarboxylative Mono- and gem-Difluorination of Malonic Acid Derivatives. J. Am. Chem. Soc 2019, 141, 5617–5622. [PubMed: 30907583]

69. Yang Y; Niu H; Xu L; Zhang H; Cai Y, Triazine Functionalized Fully Conjugated Covalent Organic Framework for Efficient Photocatalysis. Appl. Catal. B Environ 2020, 269, 118799.

70. Shen J-C; Jiang W-L; Guo W-D; Qi Q-Y; Ma D-L; Lou X; Shen M; Hu B; Yang H-B; Zhao X, A Rings-in-Pores Net: Crown Ether-Based Covalent Organic Frameworks for Phase-Transfer Catalysis. Chem. Commun 2020, 56, 595–598.

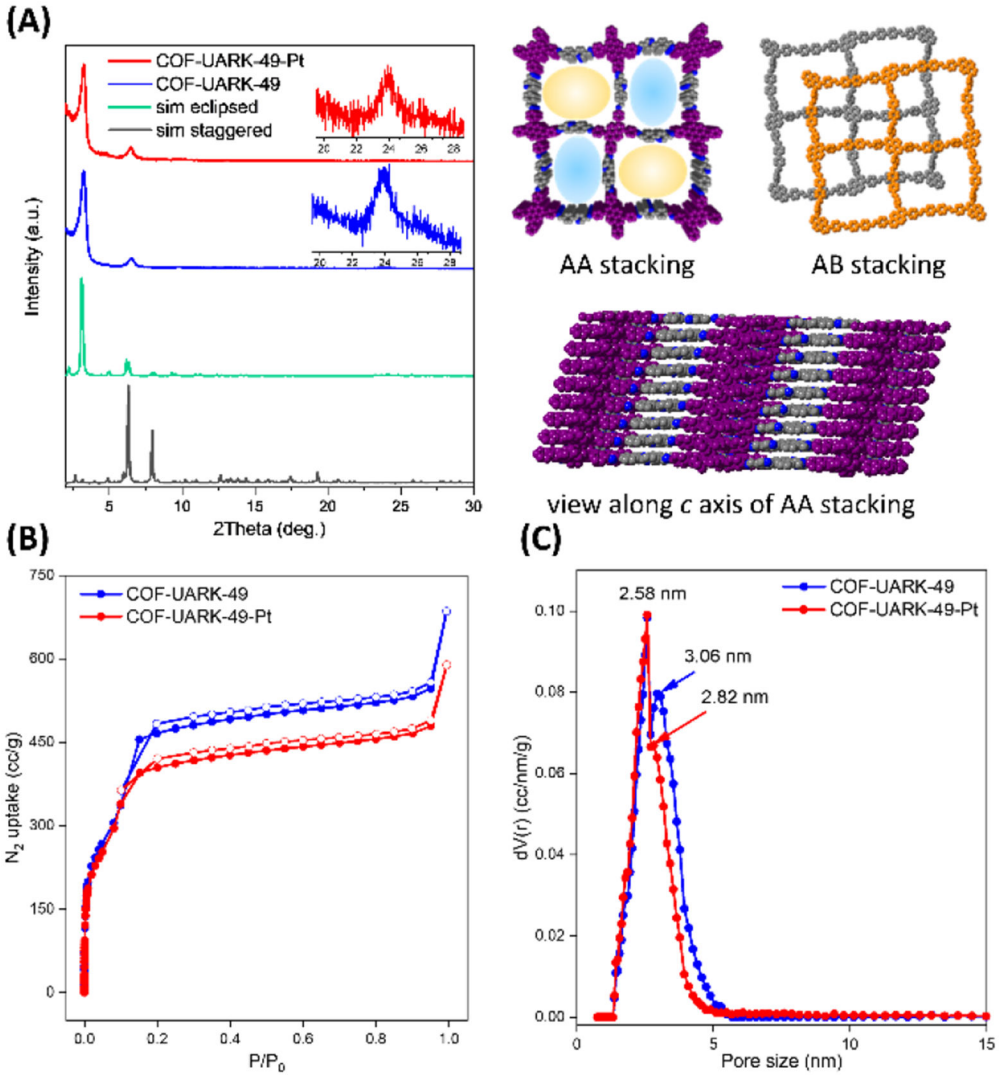

Figure 1.

(A) PXRD pattern of COF-UARK-49-Pt (red line), COF-UARK-49 (blue line), with the simulated patterns for eclipsed (green line) and staggered (gray line) stacking; (B) N_2 isotherms at 77K; and (C) Pore size distribution.

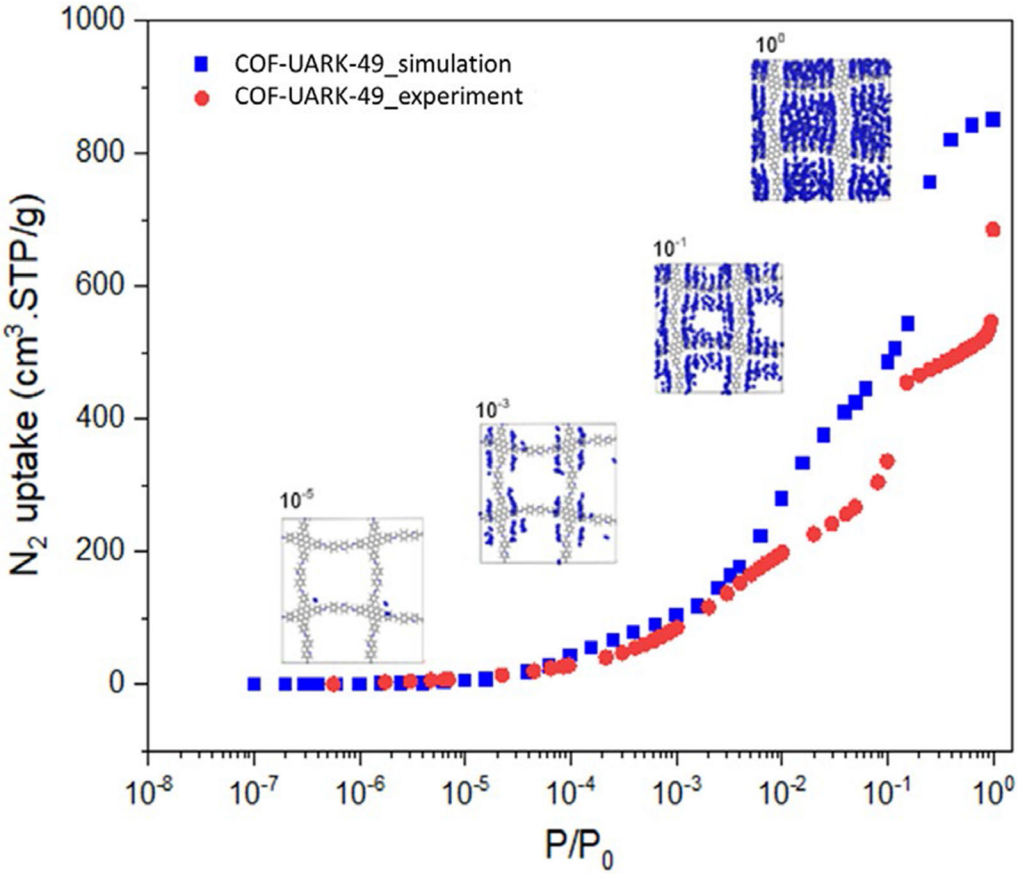

Figure 2.

Comparison of experimental and simulated N_2 uptake for COF-UARK-49. N_2 favorable adsorption sites at different pressures are shown in the inset. Blue spheres represent N_2 molecules. Framework atoms are shown in ball and stick representation.

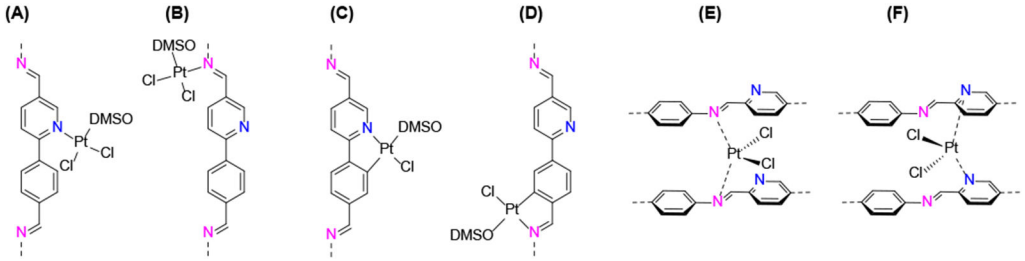

Figure 3.
(A–F) Possible coordination modes of Pt in COF-UARK-49-Pt (isomers are not shown).

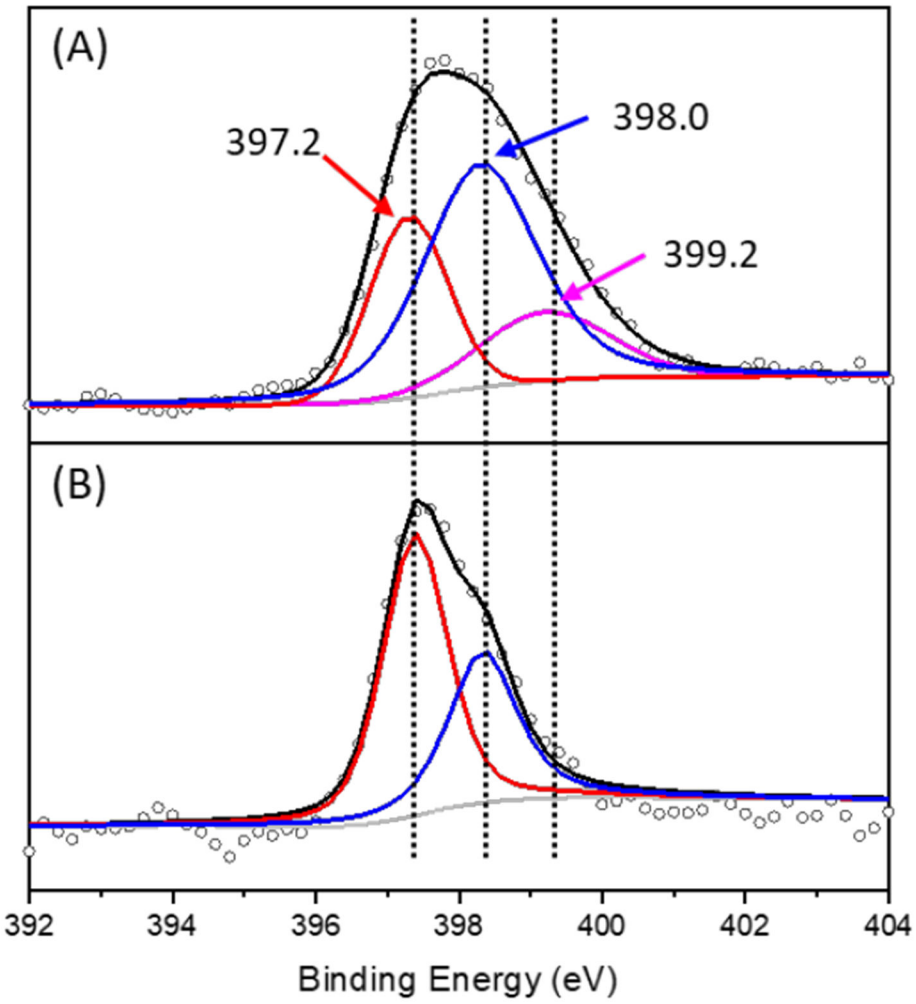

Figure 4.
XPS spectra of the N1s binding energy of (**A**) COF-UARK-49-Pt, (**B**) COF-UARK-49.

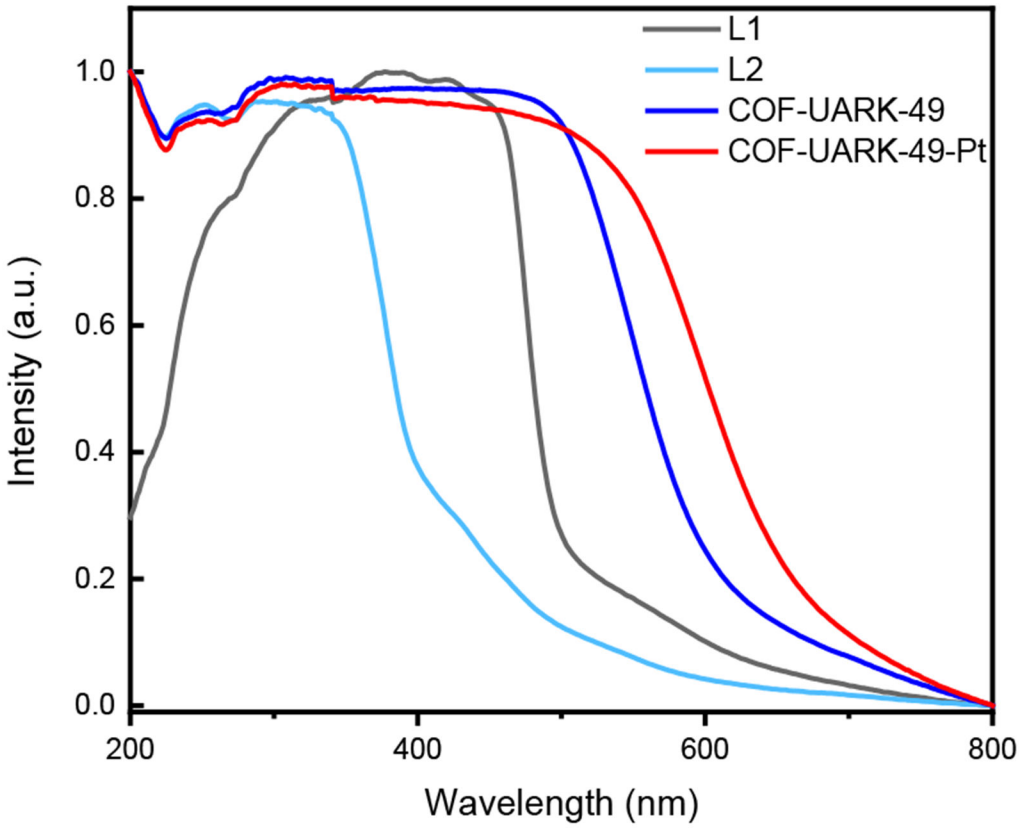

Figure 5.
Solid-state UV-vis absorption spectra of two linkers, COF-UARK-49 and COF-UARK-49-Pt.

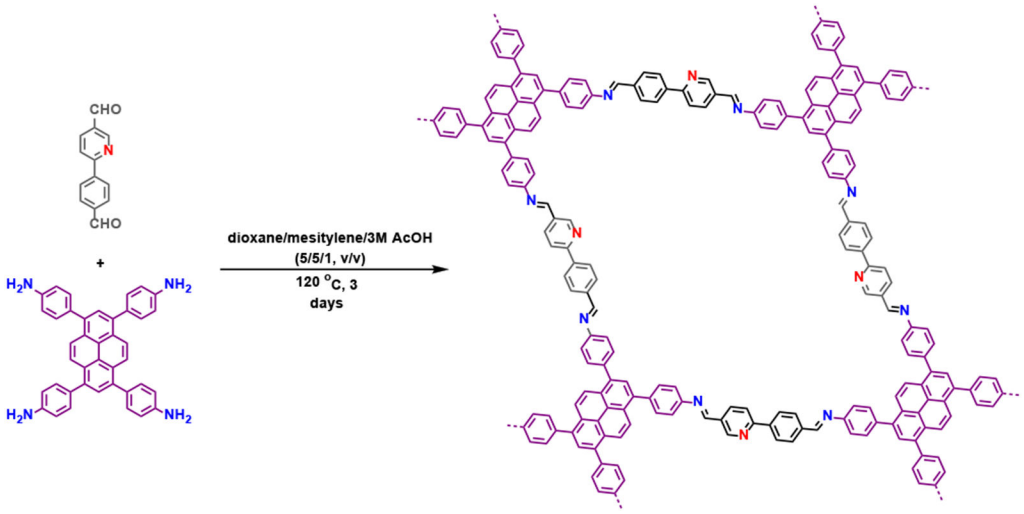

Scheme 1.
Synthesis of COF-UARK-49 via imine condensation.

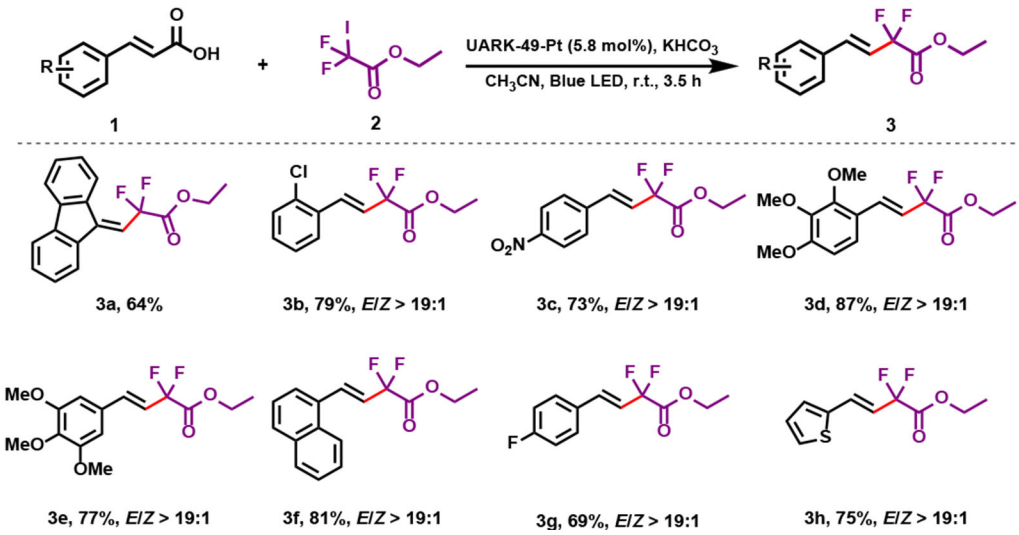

Scheme 2.
Substrate scope of decarboxylation-difluoroalkylation.

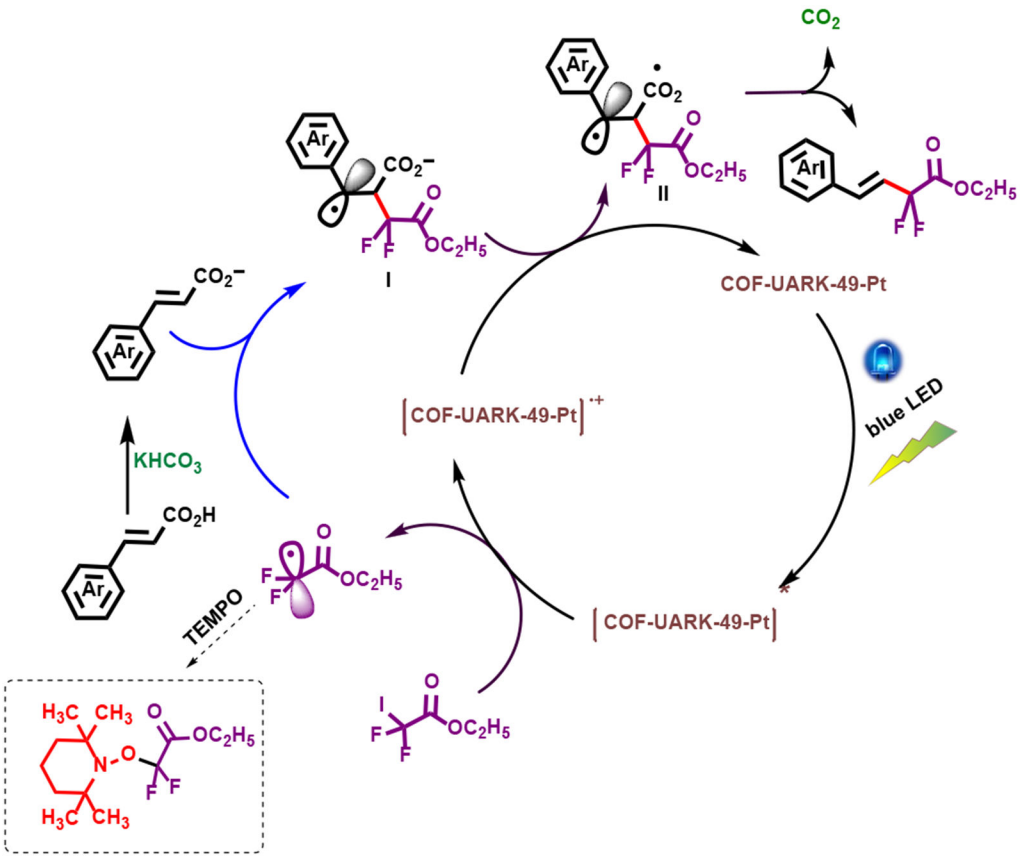

Scheme 3.
Proposed mechanism for the decarboxylation-difluoroalkylation reaction.

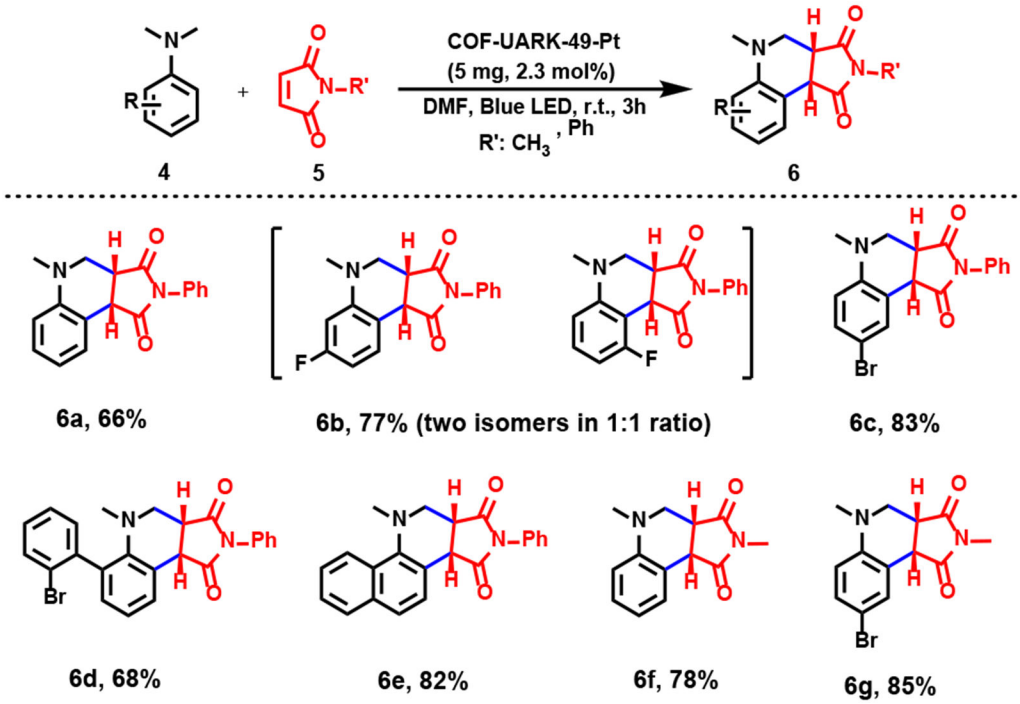

Scheme 4.

Photo-induced oxidative cyclization reaction catalyzed by COF-UARK-49-Pt.[a]

[a] A mixture of **4** (0.2 mmol) and **5** (0.1 mmol) in 1 mL DMF were illuminated with a blue LED light for 3 h in the presence of 5 mg (2.3 mol% based on Pt) of the catalyst. Yields were determined by HPLC.

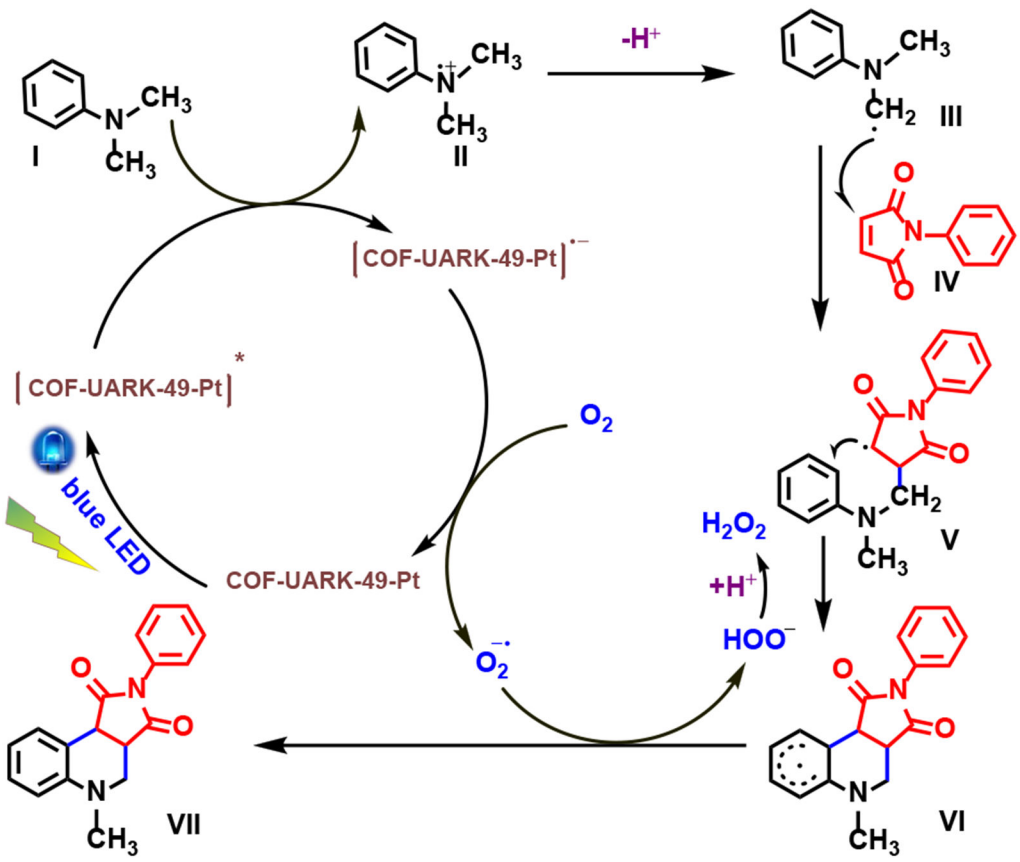

Scheme 5.
Proposed mechanism for the photo oxidative cyclization reaction

Table 1.

Optimization conditions of the reaction for the photo-induced decarboxylation-difluoroalkylation. [a]

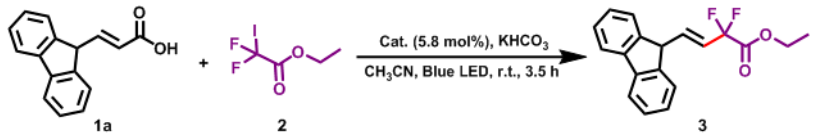

1a 2 3

Entry	Cat.	Yield (%)
1	None	<2
2	COF-UARK-49-Pt	64
3	COF-UARK-49	23
4[b]	COF-UARK-49-Pt	0
5	[$PtCl_2$(pyridine)(DMSO)]	7

[a] **1a** (0.04 mmol), **2** (0.044 mmol), $KHCO_3$ (0.044 mmol), CH_3CN (1 ml) in the presence of 5 mg (5.8 mol% based on Pt) catalyst. Yields were determined by HPLC.

[b] In dark.